Ultrafast Excited-State Proton Transfer in 4-Nitrocatechol: Implications for the Photochemistry of Nitrophenols

Avery B. Dalton[a*], *Dmitry A. Fishman*[a], *and Sergey A. Nizkorodov*[a]

[a]Department of Chemistry, University of California, Irvine, Irvine, CA 92697

Abstract

Nitrophenols are a class of environmental contaminants that exhibit strong absorption at atmospherically relevant wavelengths, prompting many studies into their photochemical degradation rates and mechanisms. Despite the importance of photochemical reactions of nitrophenols in the environment, the ultrafast processes in electronically excited nitrophenols are not well understood. Here, we present an experimental study of ultrafast electron dynamics in 4-nitrocatechol (4NC), a common product of biomass burning and fossil fuel combustion. The experiments are accompanied by time-dependent quantum mechanical calculations to help assign the observed transitions in static and transient absorption spectra, and to estimate the rates of singlet-to-triplet intersystem crossing. Our results suggest that electronic triplet states are not efficiently populated upon 340 nm excitation as efficient proton transfer occurs in the excited state on a time scale of a few picoseconds in water and tens of picoseconds in 2-propanol. This suggests that triplet states do not play a significant role in the photochemical reactions of 4NC in the environment and, by extension, nitrophenols in general. Instead, consideration should be given to the idea that this class of molecules may serve as strong photoacids.

Introduction

Nitrophenols and their derivatives, especially 4-nitrocatechol (4NC), have been identified as some of the strongest chromophores within various types of light-absorbing organic aerosols in the atmosphere (also known as "brown carbon").[1–13] In atmospheric samples, the reported mass concentrations for 4NC may exceed those of other nitrophenols by factors from ten to one hundred.[14,15] Laboratory studies of organic aerosol produced from common anthropogenic molecules such as benzene and toluene have also been shown to yield significant amounts of 4NC.[16,17] With the environmental prevalence of 4NC, and its versatile solubility, it has become a popular model of brown carbon for laboratory studies.[3,18,19] Although the photochemistry of 4NC has been studied before, the mechanisms behind the excited-state dynamics that take place in photochemical reactions of *para*- nitrophenols, such as 4NC, are not as fully explored as their *ortho*- nitrophenol counterparts.[20–25]

Photochemistry of nitrophenols and other nitroaromatics is commonly assumed to proceed through the excited triplet state manifold,[25–27] based on the notion that they would exhibit similar photochemical characteristics to nitrobenzene.[28] The earliest studies of nitrobenzene identified photoreduction products from photochemistry conducted in alcohol solutions, namely 2-propanol, with evidence of hydrogen abstraction from 2-propanol as the likely reaction pathway.[29–31] Similar conclusions have been extrapolated to many other nitrobenzene derivatives.[32–34] No studies, however, have been able to definitively prove that the degradation of 4NC occurs via a direct reaction of its triplet state, leaving a possibility that photodegradation could occur through some other pathway such as charge or proton transfer in the excited singlet state manifold.[35]

Though the ultrafast dynamics have not been studied in 4NC specifically, relevant experiments have been done with nitrophenol isomers, predominately 2-nitrophenol. Takezaki *et al*. used a transient grating approach to observe sub-nanosecond transient signals in 2-nitrophenol, assigned to its triplet state, and finding quantum yields for singlet-to-triplet intersystem crossing (ISC) ≥ 0.86 for 2-, 3-, and 4-nitrophenol in a nonpolar solvent.[28] A study by Ersnt *et al.* using time-resolved photoelectron spectroscopy on 2-nitrophenol supported previous observations by Takezaki *et al.* and determined triplet state lifetimes of 0.1 ns and 0.5 ns in 2-propanol and in n-hexane, respectively.[20] Leier *et al.* studied electron dynamics of 4-nitrophenol in aqueous solutions using conventional ultrafast transient absorption spectroscopy and found that the excitation to the lowest-energy band of 4-nitrophenol results in deprotonation at sub-nanosecond timescales, even under acidic (pH = 3-5) conditions.[36] Given that the most acidic proton in 4NC is the one in the *para* position from the nitro group,[37] the occurrence of similar ultrafast deprotonation in 4NC could have implications for the photochemical degradation of this molecule in the environment.

The main goals of this work are to examine the initial steps in 4NC photochemistry and study the effect of solvent on these processes. To this end, we have studied 4NC in both water and 2-propanol by means of ultrafast transient absorption spectroscopy over a broad spectral range. Experiments are accompanied by quantum chemical calculations using time-dependent density function theory (TDDFT) to determine and confirm the origins of the observed transients. We show that the excited 4NC undergoes a rapid proton transfer in both water and

in 2-propanol, with only a small fraction of photoexcited 4NC relaxing in the triplet state. As a result, photoexcited 4NC is not expected to react through the triplet state and instead may behave as a photoacid on picosecond timescales.

Materials and Methods

Experimental Methods

Transient absorption spectroscopy experiments were conducted with 0.6 mM solutions of 4NC (Acros Organics, 97%) in aqueous (Milli-Q ultrapure) and 2-propanol (Fisher, HPLC grade, 99.9%) solutions in a 2 mm quartz cell (Starna Cells, Spectrosil). The experiments were performed in standard non-collinear pump–probe fashion. The fundamental pulse at 800 nm (100 mW, 1 kHz) was partially focused on a CaF_2 plate to generate a white-light continuum for use as the probe pulse. Output of the femtosecond amplified system (Spitfire Ace, Spectra-Physics, MKS Instruments) was coupled to an optical parametric generator/amplifier to produce a 680 nm pulse, converted by a BBO crystal to 340 nm (0.5 mW) that was utilized as the pump beam. The time delay between pulses was scanned by a delay line (Newport, MKS Instruments), and the transient signal at each spectral component was recorded with a CCD-equipped spectrometer (Oriel, Newport, MKS Instruments). Excitation conditions generated transient signals that were confirmed to be in a linear regime for the detector response. The data indicate a probe pulse chirp of 500 fs mainly affecting wavelengths below 500 nm due to third-order nonlinear dispersion in CaF_2 crystal. This limits the possibility of quantitative analysis of the initial sub-picosecond dynamics, i.e., rise and build up of the transient signals, but does not affect interpretation of processes occurring on a picosecond timescale.

The data presented in this work are from solutions which were air saturated and analyzed without any alteration of the intrinsic pH. Although the presence of dissolved oxygen could reduce the observed triplet state yields, the effects of energy-transfer to oxygen is expected to be minimal for short-lived triplets.[30] We confirmed, there are no appreciable indicators of signal arising from reactions with dissolved oxygen from a trial after purging with N_2. Static absorption spectra of the same solutions were collected using a Shimadzu UV-2450 spectrophotometer.

Computational Methods

The Q-Chem 5 quantum chemistry package was used in for the theoretical calculations in this work.[38] Geometry optimizations and TDDFT calculations were performed using the PBE0 hybrid exchange functional and the Pople 6-311+G(d)basis set.[39,40] Other functionals were tried, such as CAM-B3LYP, X3LYP, and M06-2X, however PBE0 produced vertical excitation energies which had excellent agreement with the experimental spectra. The initial geometric configuration chosen to optimize was chosen based on the most stable conformer from Cornard *et al*.[37] The conductor-like polarized continuum model (C-PCM) was used to account for solvation, with the default specifications used in Q-Chem. Simulated excitation spectra were produced using Gaussian distributions for each spectral line with FWHM = 43 nm.

Orbital analysis was done with the generation of Natural Transition Orbitals (NTOs) in Q-Chem. The Alpha NTOs calculated within the random-phase approximation were visualized in IQmol at a contour value of 0.05 $Å^{-3}$. From the character of the orbitals in these orbital images, inferences were made toward the most probable ISC partners. The rates of ISC, k^n_{ISC},

between the first excited singlet state, S_1, and the lower energy triplet states T_n (n=1-3) can be expressed using Fermi's golden rule.[41]

$$k_{ISC}^{n} = \frac{2\pi}{\hbar}\left|\langle \Psi_{S_1}(Q_0)|\hat{H}_{SO}|\Psi_{T_n}(Q_0)\rangle\right|^2 \cdot \rho(\Delta E, \lambda, T) \quad (1)$$

A similar method was previously employed for 2- and 4-nitrophenol.[42] The bracketed term is the square of the spin-orbit coupling (SOC) matrix elements, which can be calculated directly in Q-Chem. $\rho(\Delta E, \lambda, T)$ is the Franck-Condon (FC) weighted density-of-states,

$$\rho(\Delta E, \lambda, T) = \frac{1}{\sqrt{4\pi k_B T \lambda}} \exp\left(\frac{-(\Delta E+\lambda)^2}{4\lambda k_B T}\right), \quad (2)$$

where ΔE represents the energy difference between S_1 and T_n at their respective nuclear coordinates, and λ (often referred to as the reorganization energy) is the relative energy of the T_n state at the nuclear coordinates of the S_1 state. All calculations were performed at T = 300 K. Values for ΔE and λ were obtained by geometry optimization of the TDDFT excited states, in which the Tamm-Dancoff Approximation (TDA) needed to be used to overcome issues with imaginary roots in full TDDFT optimizations. Though TDDFT has been shown to work well with small molecules, it is recognized that the accuracy of TDDFT in determining the geometries of excited states is less accurate than coupled-cluster singles and doubles (CCSD).[43,44] It is also recognized that full TDDFT often underestimates the stability of charge-transfer (CT) states, which are present in nitroaromatics,[27,45,46] though use of TDA may help in this regard.[47,48] If CT states are present in 4NC, the incurred errors will be directly dependent on the amount of CT character for each state.[49]

Results and Discussion

Indications from theoretical calculations

Figure 1 shows the measured static absorption spectrum of 4NC overlaid with the result from the ground-state TDDFT simulation. The experimental and modeled absorption spectra are in good agreement in terms of both the peak positions and overall shape, as demonstrated in the Figure 1 inset using the second derivatives of the spectral data. The best match to experimental observations has been achieved using PBE0/6-311+G(d) for modeling. The peaks at 347, 299, and 230 nm are assigned to transitions into S_1, S_3 and S_5 states, respectively. Transitions into S_2 and S_4 are not visible due to their negligibly small oscillator strengths predicted by the calculations. The extended data set of the molecule's energy structure and the oscillator strengths for transitions from S_0 into states up to S_{10} are presented in Table S1. In addition, Table S2 provides relative vertical excitation energies for potential transitions originating from the S_1, T_1 and T_3 states, covering possible transitions within the experimental spectral range.

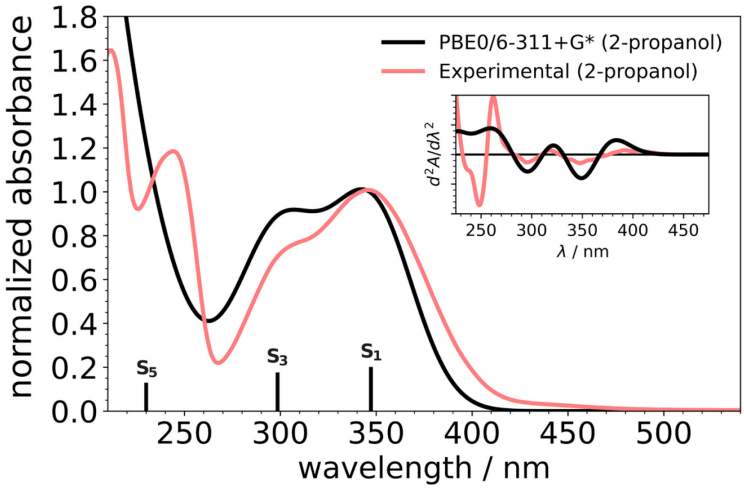

Figure 1. Simulated absorption spectrum for 4-nitrocatechol at the TD-PBE0/6-311+G(d) level of theory (black trace) compared to the experimental absorption spectrum (red trace). The experimental spectrum was collected in 2-propanol, and the simulated spectrum employed C-PCM to mimic such conditions. The spectra are normalized to the peak value of the lowest-energy band at 347 nm.

The potential energy diagram in Figure 2 (Fig. S1 for water) was used to identify starting coordinates for excited-state geometry optimizations, keeping in mind the -NO_2 group in excited-state nitroaromatics often exhibits a twisted form.[45,50–52] Accordingly, Figure 2A shows that S_1 energy is reduced by twisting the -NO_2 group, which is especially noticeable at torsion angles greater than 50°. The S_1 state energy is minimized further by the pyramidalization of the -NO_2 group as shown in Figure 2B. The obtained angles at the minimum for each state were used for the initial step of TDDFT/TDA excited-state geometry optimizations. SOC constants for $S_1 \rightarrow (T_1\text{-}T_5)$ are shown as a function of torsion and pyramidalization in Figure 2C and 2D. It is important to note that in Q-Chem the labels of each state do not account for energetic crossings and reset to the ordering of states at each TDDFT/TDA calculation. Energetic rearrangement of states may be the cause of large variations in SOC constants in 2D. The optimized geometries of each state are provided in the Supporting Information (SI).

The SOC constants and the corresponding k^n_{ISC} values estimated using Eq. 1 are provided in Table 1. The strongest coupling is obtained for S_1-T_3 states. This follows nicely El-Sayed's rules,[53] as analysis of the natural transition orbitals (NTOs, Fig. S2) predicts ππ* and nπ*characters for S_1 and T_3, respectively. The rate constant for $S_1 \rightarrow T_1$ is negligibly small, which is common for states with large energy differences when using a Gaussian distribution in $\rho(\Delta E, \lambda, T)$.[54] While the S_1-T_3 transition is expected to be the fastest, the estimated ISC rate constant for $S_1 \rightarrow T_3$ too low resulting in a long lifetime ($\tau \approx 27$ ns) that far exceeds a timescale observable with the ultrafast methods in this work. It is important to note that the use of Eq. 1 relies on the Condon approximation, which assumes that there is a negligible change in the electronic coupling with geometric reconfiguration between initial and final states.[55] It is clear from Figure 2C that the Condon approximation alone is not enough to estimate electronic coupling. This is also evident from smaller than expected k^n_{ISC} values in Table 1, especially for

T_1 and T_2. Further computational studies could evaluate the inclusion of second-order spin-orbit coupling elements toward achieving more accurate ISC rate estimates for this system.[56,57]

Although not evident in the FC excitations, a deeper analysis of the NTOs in Fig. S3 reveals the development of twisted intramolecular charge transfer (TICT) character as 4NC assumes the S_1 geometry. Despite working well for the electronic structure from the ground state, PBE0 could ultimately fail to estimate the stability of the CT states. The Coulomb-attenuated functional CAM-B3LYP has been shown to yield significant improvements toward predicting the properties of CT-type molecules.[58–60] With this in mind the aforementioned calculations with PBE0 were also done with CAM-B3LYP and the analogous results are shown in Fig. S4 and S5 with and without TDA, respectively. Interestingly, the FC excitation of $S_0 \rightarrow S_1$ is blue-shifted nearly 40 nm compared to experimental observations and what is predicted by PBE0. Optimization of S_1 with CAM-B3LYP does also favor the TICT form, which is again higher in energy compared to PBE0. Rough estimates of k^n_{ISC} from the triplet-state minima in Fig. S4 and Fig. S5 yield ISC rate constants effectively equivalent to those PBE0 (Table S4). In summary, it seems the choice of the functional does not result in significant changes in the ISC rate constant estimation. As will become apparent in the following sections, it seems that this framework for estimating ISC rate constants fails for 4NC.

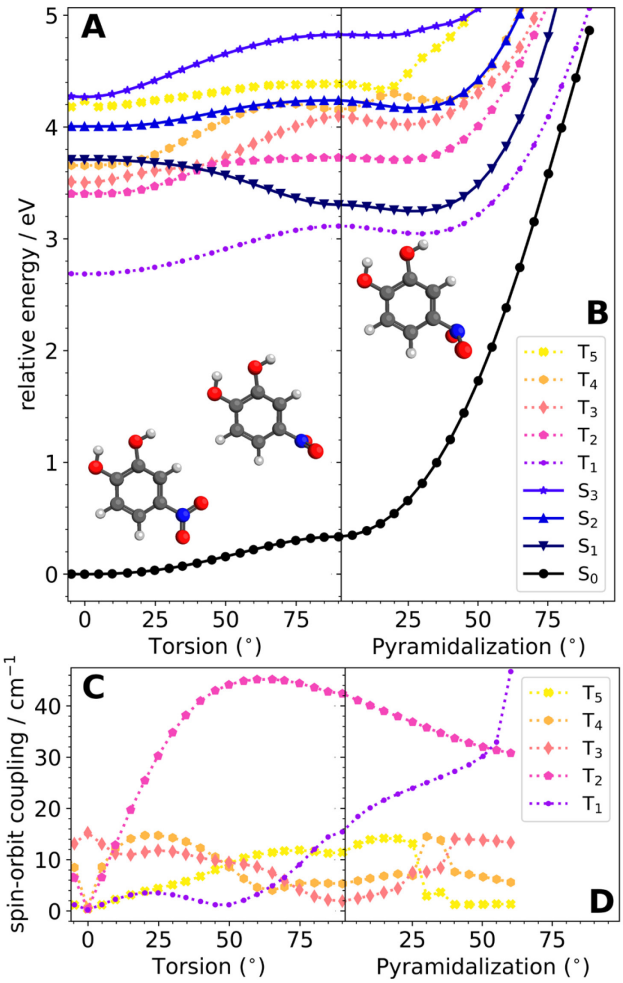

Figure 2. The effects of torsion and pyramidalization of the -NO_2 group in 4-nitrocatechol, starting from the ground-state geometry. The total energy for each state (S_0-S_3 and T_1-T_5) are shown in panels A and B and the spin-orbit coupling constants for $S_1 \rightarrow T_{1\text{-}5}$ are shown in panel C and D, as calculated at the TD/TDA-PBE0/6-311+G(d) level with a CPCM for 2-propanol.

Table 1 Spin-orbit coupling constants (TD-PBE0/6-311+G(d)) and estimated rate constants for intersystem crossing for S_1 to T_n transitions of 4-nitrocatechol in 2-propanol

Transition ($S_1 \rightarrow T_n$)	Spin-orbit coupling constant / cm^{-1}	k_{ISC} ($S_1 \rightarrow T_n$) / s^{-1}
T_1	0.268	2.40×10^{-1}
T_2	0.563	3.57×10^{2}
T_3	13.7	3.65×10^{7}
Note: energetic quantities used to calculate k are provided in Table S3		

Identification of transient signals

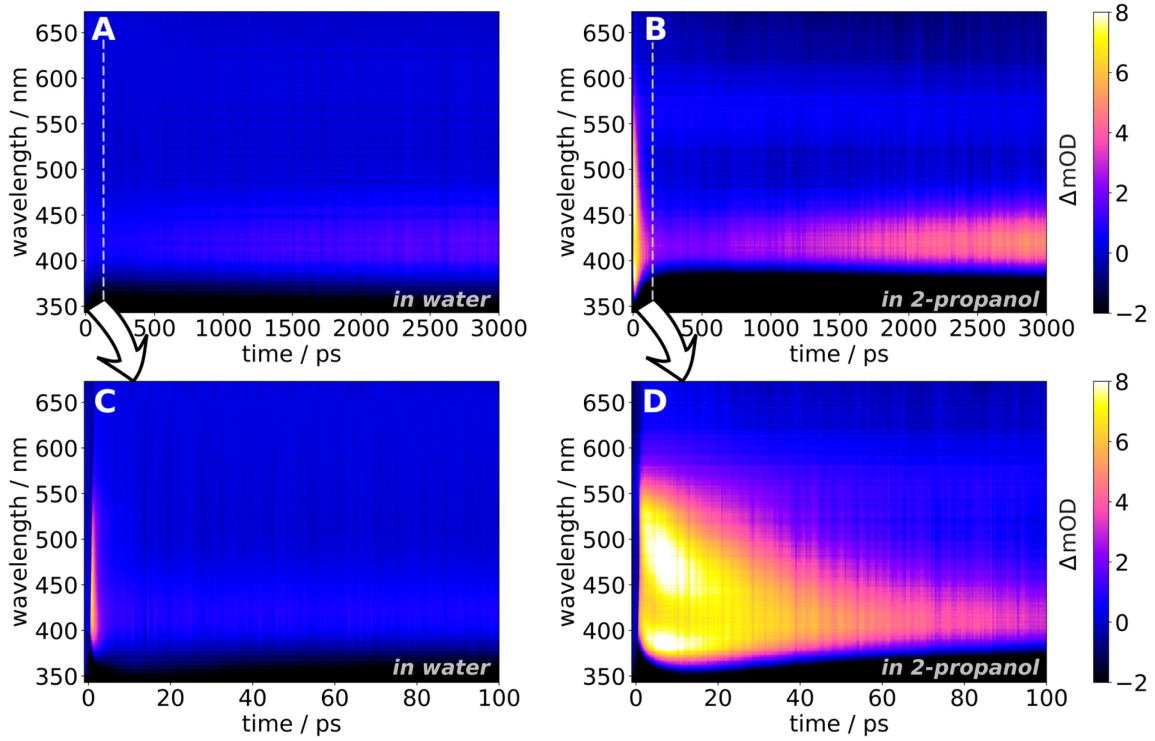

Figure 3. Transient absorption contour plots of 4-nitrocatechol pumped at 340 nm. Panels A and C show the full experimental time trace collected over 3000 ps, illustrating the rise of signal between 400 and 450 nm. Panels B and D are zoomed in on the first 100 ps of the ultrafast signal.

The transient absorption spectra obtained from 4NC in water and 2-propanol are shown as a false color map in Figure 3. Figures 3A and 3B show transient absorption (ΔmOD) for the full 3000 ps measured after the excitation, while Figures 3C and 3D are focused on the initial 100 ps time dynamics. There is a striking difference between the transient signals in 2-propanol and water – the transients in water are shorter-lived than in 2-propanol.

Figure 4A-C shows dynamics for 4NC in water. The transient signal build-up occurs in under 1 ps at 440 nm. The absorption features at these timescales are likely the result of twisted intramolecular charge transfer (TICT), which indeed should occur at sub-picosecond timescales in other nitroaromatics.[52] The presence of an isosbestic point at 510 nm in Figure 4A (blue/violet traces) is indicative that the sub-picosecond state converts into a new state manifesting itself as a broad absorption band from 400 nm to 600 nm. This absorption feature dissipates within the next 10 ps reaching a steady plateau (Figure 4C). The sustained signal has a resemblance to the observations for 4-nitrophenol, a structurally similar molecule to 4NC, by Leier *et al*., where a similar absorption spectrum at longer time scales has been assigned to the anion of 4-nitrophenol.[36] Hence, we hypothesize that this new state could be a result of intermolecular excited-state proton transfer (ESPT) from 4NC to the solvent. This is of particular interest, as these signals appear not only in water but also in less polar 2-propanol.

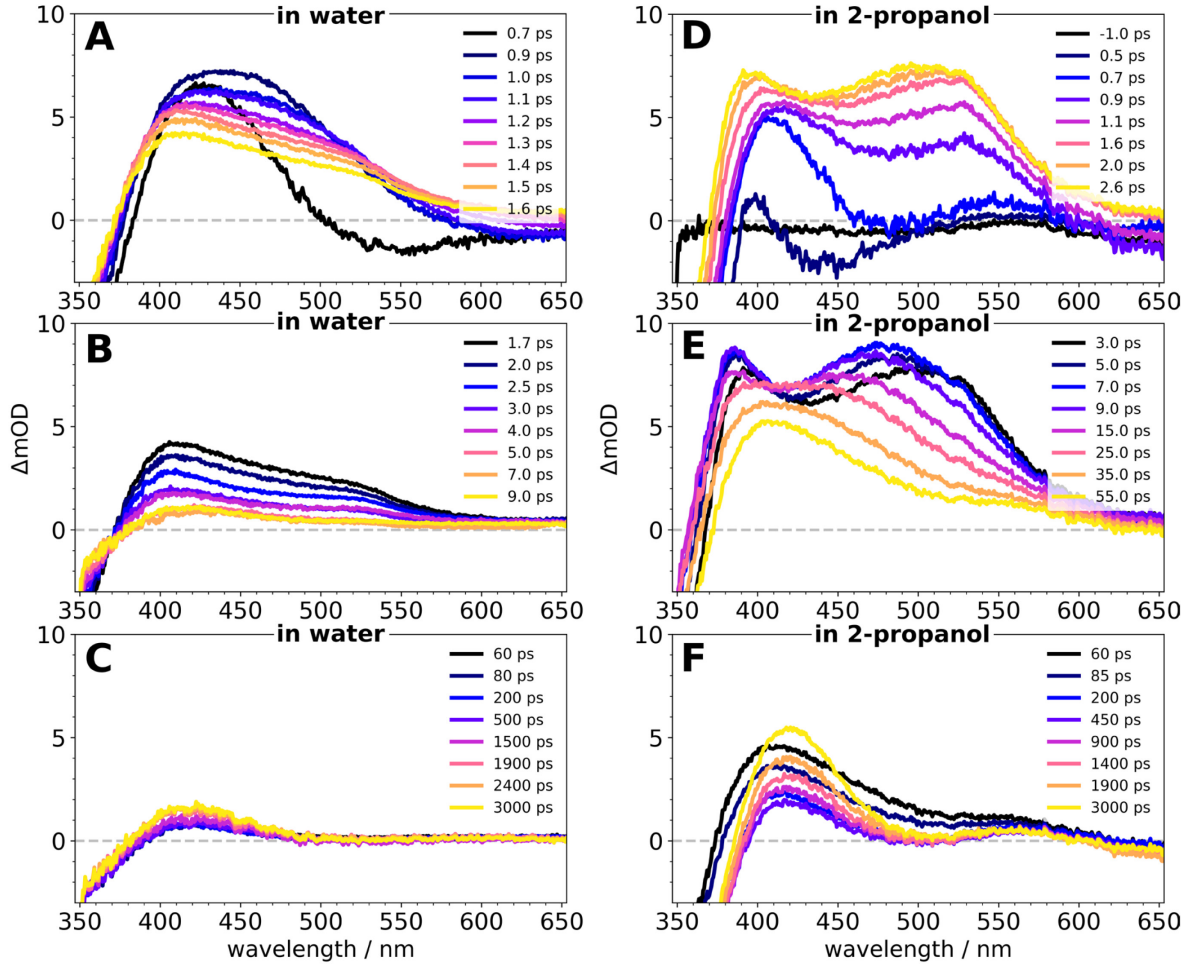

Figure 4. Individual transients observed at various times during the ~3 ns experiment. The time intervals for each subpanel were chosen in an attempt to highlight the unique spectra which appear at different times. Panels A, B, and C are data from aqueous experiments, and panels D, E, and F are data from 2-propanol experiments. The delay times are indicated in each panel by trace color.

The spectral evolution for 4NC in 2-propanol is shown in Figure 4D-F. Again, the TICT appears to be present at early delay times. In contrast to the spectral dynamics in aqueous

solution, a new excited-state absorption band (yellow curve in Fig. 4D) is formed in a few picoseconds, which is likely the result of rapid $S_1 \rightarrow T_n$ ISC after the reorientation of the $-NO_2$ group. This underlines an important difference between the aqueous and organic solvents, as ISC did not seem to occur in the former. The theoretical calculations suggest that the ISC destination is either T_1 or T_2, though this is difficult to confirm experimentally. Following ISC, the excited-state absorption within the triplet manifold (Fig. 4E) evolves toward an absorption band similar to the one that appeared between in water (Fig. 4B). This absorption feature decays with $\tau \approx 58$ ps in 2-propanol and $\tau \approx 2$ ps in water. Most likely it corresponds to excited-state absorption by a higher excited state in the anion, which we will denote as X_*^- in Figure 5. This further confirms the notion that signals at longer times (420 nm, 3 ns) appear to be associated with similar chemical species in both solvents.

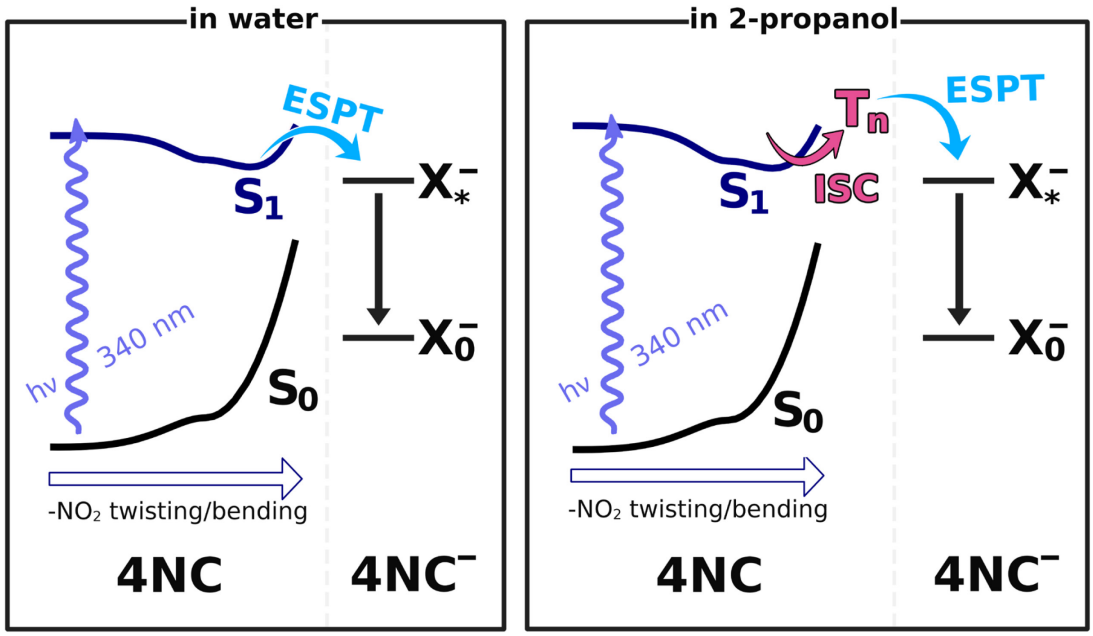

Figure 5. Schematic diagram representing the solvent-dependent excited state dynamics observed with 4NC. The left shows 4NC undergoing ESPT while still in a singlet state in water, and the right shows 4NC first going through ISC prior to ESPT.

To support our conclusions about facile ESPT in 4NC, Figure 6 shows transient spectra at 3 ns in both solvents overlayed with the static absorption spectra of singly- and doubly-deprotonated 4NC recorded in water. The static spectra were measured by titrating aqueous 4NC with potassium hydroxide, and the spectrum pH dependence is shown in Figure S6. The mono-deprotonated anion of 4NC, or $4NC^-$, has a maximum in the same region at 425 nm. Assuming $4NC^-$ is being formed in both solutions, the slower-evolving transient signal being observed in 2-propanol is not surprising. Water is a much more efficient acceptor for excited-state intermolecular proton transfer than alcohols, leading to a significantly faster transfer.[61] It is important to note that the spectra at 3 ns in both solvents are a result of a gradual rise over more than 2 ns in both solvents. This rise is evident in the time profiles provided in Figure S7.

The linear nature of these rising absorption signals suggests that it may not be dynamics; instead, it appears that it may be the result of a building up of the anion in solution over the course of the experiment.

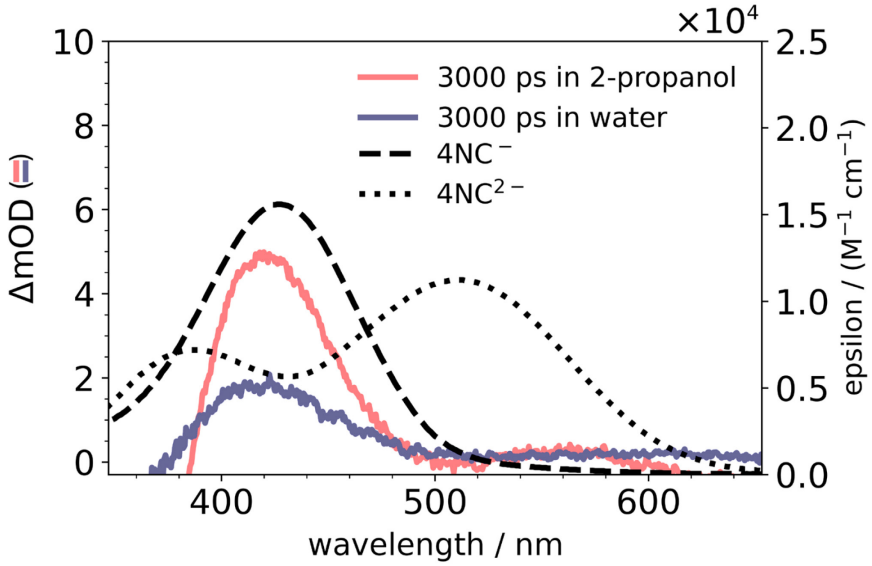

Figure 6. Overlayed spectra of the long-lived transient absorption signal in 2-propanol (salmon) and water (violet) on the left axis with the extinction spectra of the mono- (dashed) and doubly- (dotted) deprotonated forms of 4NC on the right axis.

Ultrafast rates of ISC and ESPT

Figure 7 compares the time dynamics for 4NC in 2-propanol and water, at the probe wavelengths roughly corresponding to the appearance and subsequent disappearance of excited-state absorption. The data have been fitted using single exponential functions with time constants being reported in Table 2. We note, it is not possible to precisely determine time constants for each transformation due to the strong overlap of their broad spectral lines. With absorption by X_*^- overlapping (yellow trace in Fig. 4E) with the signal by T_n (475 nm, black/blue traces in Fig. 4E), the decay lifetime reported for T_n would be an upper limit for the transition from T_n to X_*^-. At 525 nm, the signal decays with a time constant $\tau \approx 24$ ps, perhaps a better estimate for the timescale of ESPT in 2-propanol. The only transient signal that can be quantitively analyzed for 4NC in water is associated with X_*^- decay within 1.7 ps, which effectively represents the overall transient response. As such times are exceedingly short for spin forbidden transitions, we hypothesize, ESPT is a primary mechanism of decay and occurs in both solvents on ultrafast timescales.

Table 2 Wavelengths of maximum change in absorbance and effective lifetimes of transient processes in 4-nitrocatechol

Species	**Description**	**Maximum ΔOD Wavelength**	**τ_{decay} / ps**

2-propanol			
TICT S_1	Neutral excited state	405 nm	n.d.[a]
T_n	Neutral excited state	475 nm	36 ± 1
X^-_*	Anion excited state	405 nm	58 ± 2
water			
TICT S_1	Neutral excited state	440 nm	n.d.
X^-_*	Anion excited state	405 nm	1.7 ± 0.1

[a]These lifetimes were not determined due to the overlapping of absorption signals or too rapid change. The uncertainty provided is a 95% confidence interval from the fit.

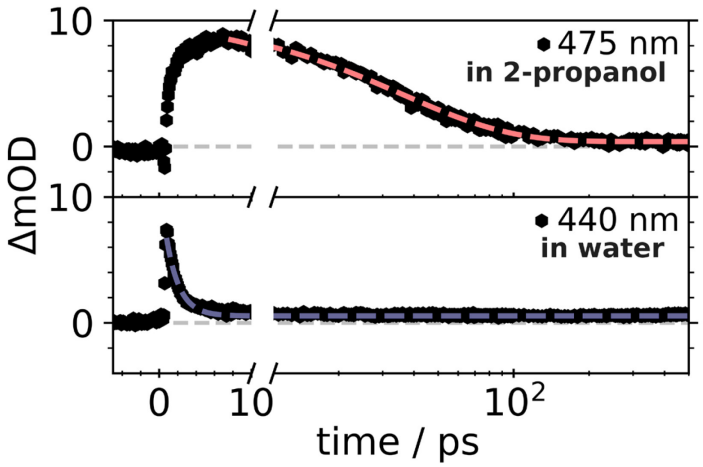

Figure 7. Transient absorption traces the longest-lived triplet signals by 4NC in 2-propanol (top) and water (bottom). The broken x-axis is used to illustrate the rapid decay of the triplet state. The left x-axes show the initial rise of signal within 10 ps. The overlayed dashed lines are the results of fitting the signal, as described in the SI.

The striking contrast in time scales of the ESPT process in aqueous and 2-propanol solutions (Figure 7) is clear. Due to the complexity of transient spectrum and significant overlap of the broad absorption bands, the ESPT rates cannot be precisely determined from the current experimental data. However, a rough estimate can be made based on decay times at 405 nm (~2 ps), putting the ESPT rate constant at ~5×10^{11} s^{-1}. This ultrafast rate approaches what is believed to be the upper limit of ESPT rates at ~10^{13} s^{-1} reported previously.[62–64] Since water is a much more effective base than 2-propanol, it allows for ESPT to occur almost immediately after the TICT. In contrast, the lag in ESPT in 2-propanol allows for ISC to the triplet manifold to take place, after which the ESPT occurs from a triplet state.

The transient absorption signals at 550-600 nm range do not fully vanish within 3 ns, suggesting a small population remains in a triplet state. In previous work on broadband photochemical degradation of 4NC in 2-propanol,[35] it was believed triplet 4NC would decay by abstracting a hydrogen atom from 2-propanol. The observed effective photochemical degradation yield was found to be ~10^{-5} for the loss of 4NC in 2-propanol. This suggests that either the triplet state has a low quantum yield, or it is not reactive with the solvent. The

energies of the T_1 (2.6 eV), T_2 (3.1 eV), and T_3 (3.4 eV) states are lower than the C-H bond energy (4 eV), hence the presence of the energy potential barriers is also likely to limit such a process. If due to the dominant ESPT process only a small fraction of the excited molecules remains at the triplet state, this would explain relatively slow, yet observable, photodegradation in 4NC.

Ultrafast time scales of ESPT in 4NC indicate the role of triplet states toward the environmental photochemistry of 4NC and other nitrophenols may be minimal. Some studies have identified nitrosophenol compounds as potential intermediates in the photodegradation of nitrophenols,[34,35,65,66] which may be the result of an electron transfer processes following the ESPT. While nitroaromatics are often classified as having similar characteristics across the board, perhaps further delineation is necessary among these "push-pull" type nitrophenols. Nitrophenols are strong chromophores, their S_1 transitions are usually of $\pi\pi^*$ instead of $n\pi^*$ character, and they have strong indications toward being effective photoacids.

Conclusions

This work utilized transient absorption spectroscopy to compare the photophysical dynamics of 4NC in an organic environment (2-propanol) and the aqueous phase. Upon excitation at 340 nm, the S_1 state is immediately populated in both solvents. The mechanisms within the triplet manifold differ between the two solvents. In 2-propanol there are indications of ISC into a triplet state, most likely T_2 or T_3 as indicated by quantum chemical calculations. There is no ISC process apparent in the aqueous phase; instead, it appears to be an ultrafast ESPT producing ground-state 4NC anion within 10 ps. The resulting spectra at long delay times (~3 ns) in both solvents are spectrally similar to the mono-deprotonated anion $4NC^-$, indicating that ESPT happens in both solvents. Unlike in the aqueous phase, ESPT in 2-propanol takes longer as it appears to first go through a relatively short-lived $S_1 \rightarrow T_n$ conversion. Because ESPT reduces the triplet state yield, it reduces the efficiency of the photodegradation of 4NC in either aqueous or organic matrices and minimizes the probability of secondary triplet-state chemistry of 4NC.

The results in this work could have implications toward the general treatment of nitrophenol photochemistry. While there is evidence of the short-lived triplet states, it is worth considering the role that the anion could play a significant role towards condensed-phase photodegradation of 4NC. The results show 4NC has photoacidic characteristics and this conclusion is in good agreement with recent studies on 4-nitrophenol. It is worth emphasizing that the ultrafast nature of the proton transfer in 4NC appears to approach the territory of "super" photoacids, particularly in water. Further studies should be done to quantify the rate of ESPT in 4NC or other para-nitrophenols.

AUTHOR INFORMATION

Corresponding Author

* E-mail: abdalton@uci.edu

ORCID

Avery B. Dalton: 0000-0002-6923-9090

Sergey A. Nizkorodov: 0000-0003-0891-0052

Dmitry A. Fishman: 0000-0001-6287-2128

Author Contributions

The experiments and data analysis were conceived by ABD and SAN, and carried out ABD and DAF. Computational work was carried out by ABD. The manuscript was written by ABD and edited by SAN and DAF. All authors have approved the final version of the manuscript.

Notes

The authors declare no competing financial interest.

Supporting Information

Numerical TDDFT results (Table S1-S3); Energy surfaces for 4NC in water (Fig. S1); Natural transition orbitals (Fig. S2 & S3); TDDFT results for CAM-B3LYP (Fig. S4 & S5); pH-dependent 4NC absorption spectra (Fig. S6); Transient absorption at 420 nm in water and 2-propanol (Fig. S7)

Acknowledgements

This experimental work was supported by the US National Science Foundation grant AGS-1853639.

References

(1) Iinuma, Y.; Brüggemann, E.; Gnauk, T.; Müller, K.; Andreae, M. O.; Helas, G.; Parmar, R.; Herrmann, H. Source Characterization of Biomass Burning Particles: The Combustion of Selected European Conifers, African Hardwood, Savanna Grass, and German and Indonesian Peat. *Journal of Geophysical Research: Atmospheres* **2007**, *112* (D8), D08209. https://doi.org/10.1029/2006JD007120.

(2) Kahnt, A.; Behrouzi, S.; Vermeylen, R.; Safi Shalamzari, M.; Vercauteren, J.; Roekens, E.; Claeys, M.; Maenhaut, W. One-Year Study of Nitro-Organic Compounds and Their Relation to Wood Burning in PM10 Aerosol from a Rural Site in Belgium. *Atmospheric Environment* **2013**, *81*, 561–568. https://doi.org/10.1016/j.atmosenv.2013.09.041.

(3) Zhao, R.; Lee, A. K. Y.; Huang, L.; Li, X.; Yang, F.; Abbatt, J. P. D. Photochemical Processing of Aqueous Atmospheric Brown Carbon. *Atmospheric Chemistry and Physics* **2015**, *15* (11), 6087–6100. https://doi.org/10.5194/acp-15-6087-2015.

(4) Lin, P.; Liu, J.; Shilling, J. E.; Kathmann, S. M.; Laskin, J.; Laskin, A. Molecular Characterization of Brown Carbon (BrC) Chromophores in Secondary Organic Aerosol Generated from Photo-Oxidation of Toluene. *Phys. Chem. Chem. Phys.* **2015**, *17* (36), 23312–23325. https://doi.org/10.1039/C5CP02563J.

(5) Lin, P.; Aiona, P. K.; Li, Y.; Shiraiwa, M.; Laskin, J.; Nizkorodov, S. A.; Laskin, A. Molecular Characterization of Brown Carbon in Biomass Burning Aerosol Particles. *Environ. Sci. Technol.* **2016**, *50* (21), 11815–11824. https://doi.org/10.1021/acs.est.6b03024.

(6) Caumo, S. E. S.; Claeys, M.; Maenhaut, W.; Vermeylen, R.; Behrouzi, S.; Safi Shalamzari, M.; Vasconcellos, P. C. Physicochemical Characterization of Winter PM10 Aerosol Impacted by Sugarcane Burning from São Paulo City, Brazil. *Atmospheric Environment* **2016**, *145*, 272–279. https://doi.org/10.1016/j.atmosenv.2016.09.046.

(7) Iinuma, Y.; Keywood, M.; Herrmann, H. Characterization of Primary and Secondary Organic Aerosols in Melbourne Airshed: The Influence of Biogenic Emissions, Wood Smoke and Bushfires. *Atmospheric Environment* **2016**, *130*, 54–63. https://doi.org/10.1016/j.atmosenv.2015.12.014.

(8) Al-Naiema, I. M.; Stone, E. A. Evaluation of Anthropogenic Secondary Organic Aerosol Tracers from Aromatic Hydrocarbons. *Atmospheric Chemistry and Physics* **2017**, *17* (3), 2053–2065. https://doi.org/10.5194/acp-17-2053-2017.

(9) Bluvshtein, N.; Lin, P.; Flores, J. M.; Segev, L.; Mazar, Y.; Tas, E.; Snider, G.; Weagle, C.; Brown, S. S.; Laskin, A.; Rudich, Y. Broadband Optical Properties of Biomass-Burning Aerosol and Identification of Brown Carbon Chromophores. *Journal of Geophysical Research: Atmospheres* **2017**, *122* (10), 5441–5456. https://doi.org/10.1002/2016JD026230.

(10) Finewax, Z.; de Gouw, J. A.; Ziemann, P. J. Identification and Quantification of 4-Nitrocatechol Formed from OH and NO3 Radical-Initiated Reactions of Catechol in Air in the Presence of NOx: Implications for Secondary Organic Aerosol Formation from Biomass Burning. *Environ. Sci. Technol.* **2018**, *52* (4), 1981–1989. https://doi.org/10.1021/acs.est.7b05864.

(11) Vidović, K.; Kroflič, A.; Šala, M.; Grgić, I. Aqueous-Phase Brown Carbon Formation from Aromatic Precursors under Sunlight Conditions. *Atmosphere* **2020**, *11* (2), 131. https://doi.org/10.3390/atmos11020131.

(12) Kroflič, A.; Anders, J.; Drventić, I.; Mettke, P.; Böge, O.; Mutzel, A.; Kleffmann, J.; Herrmann, H. Guaiacol Nitration in a Simulated Atmospheric Aerosol with an Emphasis on Atmospheric Nitrophenol Formation Mechanisms. *ACS Earth Space Chem.* **2021**, *5* (5), 1083–1093. https://doi.org/10.1021/acsearthspacechem.1c00014.

(13) Washenfelder, R. A.; Azzarello, L.; Ball, K.; Brown, S. S.; Decker, Z. C. J.; Franchin, A.; Fredrickson, C. D.; Hayden, K.; Holmes, C. D.; Middlebrook, A. M. et al. Complexity in

the Evolution, Composition, and Spectroscopy of Brown Carbon in Aircraft Measurements of Wildfire Plumes. *Geophysical Research Letters* **2022**, *49* (9), e2022GL098951. https://doi.org/10.1029/2022GL098951.

(14) Kitanovski, Z.; Hovorka, J.; Kuta, J.; Leoni, C.; Prokeš, R.; Sáňka, O.; Shahpoury, P.; Lammel, G. Nitrated Monoaromatic Hydrocarbons (Nitrophenols, Nitrocatechols, Nitrosalicylic Acids) in Ambient Air: Levels, Mass Size Distributions and Inhalation Bioaccessibility. *Environ Sci Pollut Res* **2021**, *28* (42), 59131–59140. https://doi.org/10.1007/s11356-020-09540-3.

(15) Amarandei, C.; Olariu, R. I.; Arsene, C. First Insights into the Molecular Characteristics of Atmospheric Organic Aerosols from Iasi, Romania: Behavior of Biogenic versus Anthropogenic Contributions and Potential Implications. *Science of The Total Environment* **2023**, *877*, 162830. https://doi.org/10.1016/j.scitotenv.2023.162830.

(16) Xie, M.; Chen, X.; Hays, M. D.; Lewandowski, M.; Offenberg, J.; Kleindienst, T. E.; Holder, A. L. Light Absorption of Secondary Organic Aerosol: Composition and Contribution of Nitroaromatic Compounds. *Environ. Sci. Technol.* **2017**, *51* (20), 11607–11616. https://doi.org/10.1021/acs.est.7b03263.

(17) Klodt, A. L.; Adamek, M.; Dibley, M.; Nizkorodov, S. A.; O'Brien, R. E. Effects of the Sample Matrix on the Photobleaching and Photodegradation of Toluene-Derived Secondary Organic Aerosol Compounds. *Atmospheric Chemistry and Physics* **2022**, *22* (15), 10155–10171. https://doi.org/10.5194/acp-22-10155-2022.

(18) Hems, R. F.; Abbatt, J. P. D. Aqueous Phase Photo-Oxidation of Brown Carbon Nitrophenols: Reaction Kinetics, Mechanism, and Evolution of Light Absorption. *ACS Earth Space Chem.* **2018**, *2* (3), 225–234. https://doi.org/10.1021/acsearthspacechem.7b00123.

(19) Price, C. L.; Preston, T. C.; Davies, J. F. Hygroscopic Growth, Phase Morphology, and Optical Properties of Model Aqueous Brown Carbon Aerosol. *Environ. Sci. Technol.* **2022**, *56* (7), 3941–3951. https://doi.org/10.1021/acs.est.1c07356.

(20) Ernst, H. A.; Wolf, T. J. A.; Schalk, O.; González-García, N.; Boguslavskiy, A. E.; Stolow, A.; Olzmann, M.; Unterreiner, A.-N. Ultrafast Dynamics of O-Nitrophenol: An Experimental and Theoretical Study. *J. Phys. Chem. A* **2015**, *119* (35), 9225–9235. https://doi.org/10.1021/acs.jpca.5b04900.

(21) Grygoryeva, K.; Kubečka, J.; Pysanenko, A.; Lengyel, J.; Slavíček, P.; Fárník, M. Photochemistry of Nitrophenol Molecules and Clusters: Intra- vs Intermolecular Hydrogen Bond Dynamics. *J. Phys. Chem. A* **2016**, *120* (24), 4139–4146. https://doi.org/10.1021/acs.jpca.6b04459.

(22) Vereecken, L.; Chakravarty, H. K.; Bohn, B.; Lelieveld, J. Theoretical Study on the Formation of H- and O-Atoms, HONO, OH, NO, and NO2 from the Lowest Lying Singlet and Triplet States in Ortho-Nitrophenol Photolysis. *International Journal of Chemical Kinetics* **2016**, *48* (12), 785–795. https://doi.org/10.1002/kin.21033.

(23) Blackshaw, K. J.; Ortega, B. I.; Quartey, N.-K.; Fritzeen, W. E.; Korb, R. T.; Ajmani, A. K.; Montgomery, L.; Marracci, M.; Vanegas, G. G.; Galvan, J. et al. Nonstatistical Dissociation Dynamics of Nitroaromatic Chromophores. *J. Phys. Chem. A* **2019**, *123* (19), 4262–4273. https://doi.org/10.1021/acs.jpca.9b02312.

(24) Nitta, Y.; Schalk, O.; Kaneshima, K.; Sekikawa, T. Ultrafast Photolysis of O-Nitrophenol Studied by Time-Resolved Photoelectron Spectroscopy. *EPJ Web Conf.* **2019**, *205*, 09022. https://doi.org/10.1051/epjconf/201920509022.

(25) Nitta, Y.; Schalk, O.; Igarashi, H.; Wada, S.; Tsutsumi, T.; Saita, K.; Taketsugu, T.; Sekikawa, T. Real-Time Probing of an Atmospheric Photochemical Reaction by Ultrashort Extreme Ultraviolet Pulses: Nitrous Acid Release from o-Nitrophenol. *J. Phys. Chem. Lett.* **2021**, *12* (1), 674–679. https://doi.org/10.1021/acs.jpclett.0c03297.

(26) Xu, C.; Yu, L.; Zhu, C.; Yu, J.; Cao, Z. Intersystem Crossing-Branched Excited-State Intramolecular Proton Transfer for o-Nitrophenol: An Ab Initio on-the-Fly Nonadiabatic Molecular Dynamic Simulation. *Sci Rep* **2016**, *6* (1), 26768. https://doi.org/10.1038/srep26768.

(27) Bailey-Darland, S.; Krueger, T. D.; Fang, C. Ultrafast Spectroscopies of Nitrophenols and Nitrophenolates in Solution: From Electronic Dynamics and Vibrational Structures to Photochemical and Environmental Implications. *Molecules* **2023**, *28* (2), 601. https://doi.org/10.3390/molecules28020601.

(28) Takezaki, M.; Hirota, N.; Terazima, M. Nonradiative Relaxation Processes and Electronically Excited States of Nitrobenzene Studied by Picosecond Time-Resolved Transient Grating Method. *J. Phys. Chem. A* **1997**, *101* (19), 3443–3448. https://doi.org/10.1021/jp963095t.

(29) Ciamician, G.; Silber, P. Ueber Die Einwirkung Des Lichtes Auf Eine Alkoholische Nitrobenzollösung. *Berichte der deutschen chemischen Gesellschaft* **1886**, *19* (2), 2899–2900. https://doi.org/10.1002/cber.188601902276.

(30) Hurley, R.; Testa, A. C. Photochemical n → Π* Excitation of Nitrobenzene. *J. Am. Chem. Soc.* **1966**, *88* (19), 4330–4332. https://doi.org/10.1021/ja00971a005.

(31) Hurley, R.; Testa, A. C. Nitrobenzene Photochemistry. II. Protonation in the Excited State. *J. Am. Chem. Soc.* **1967**, *89* (26), 6917–6919. https://doi.org/10.1021/ja01002a019.

(32) A. Barltrop, J.; J. Bunce, N. Organic Photochemistry. Part VIII. The Photochemical Reduction of Nitro-Compounds. *Journal of the Chemical Society C: Organic* **1968**, *0* (0), 1467–1474. https://doi.org/10.1039/J39680001467.

(33) Hashimoto, S.; Kano, K. The Photochemical Reduction of Nitrobenzene and Its Reduction Intermediates. X. The Photochemical Reduction of the Monosubstituted Nitrobenzenes in 2-Propanol. *Bull. Chem. Soc. Jpn.* **1972**, *45* (2), 549–553. https://doi.org/10.1246/bcsj.45.549.

(34) Hinks, M. L.; Brady, M. V.; Lignell, H.; Song, M.; Grayson, J. W.; Bertram, A. K.; Lin, P.; Laskin, A.; Laskin, J.; Nizkorodov, S. A. Effect of Viscosity on Photodegradation Rates in Complex Secondary Organic Aerosol Materials. *Phys. Chem. Chem. Phys.* **2016**, *18* (13), 8785–8793. https://doi.org/10.1039/C5CP05226B.

(35) Dalton, A. B.; Nizkorodov, S. A. Photochemical Degradation of 4-Nitrocatechol and 2,4-Dinitrophenol in a Sugar-Glass Secondary Organic Aerosol Surrogate. *Environ. Sci. Technol.* **2021**, *55* (21), 14586–14594. https://doi.org/10.1021/acs.est.1c04975.

(36) Leier, J.; Michenfelder, N. C.; Unterreiner, A.-N.; Olzmann, M. Indications for an Intermolecular Photo-Induced Excited-State Proton Transfer of p-Nitrophenol in Water. *Molecular Physics* **2021**, *119* (17–18), e1975051. https://doi.org/10.1080/00268976.2021.1975051.

(37) Cornard, J.-P.; Rasmiwetti; Merlin, J.-C. Molecular Structure and Spectroscopic Properties of 4-Nitrocatechol at Different PH: UV–Visible, Raman, DFT and TD-DFT Calculations. *Chemical Physics* **2005**, *309* (2), 239–249. https://doi.org/10.1016/j.chemphys.2004.09.020.

(38) Epifanovsky, E.; Gilbert, A. T. B.; Feng, X.; Lee, J.; Mao, Y.; Mardirossian, N.; Pokhilko, P.; White, A. F.; Coons, M. P.; Dempwolff, A. L. et al. Software for the Frontiers of Quantum Chemistry: An Overview of Developments in the Q-Chem 5 Package. *J. Chem. Phys.* **2021**, *155* (8), 084801. https://doi.org/10.1063/5.0055522.

(39) Adamo, C.; Barone, V. Toward Reliable Density Functional Methods without Adjustable Parameters: The PBE0 Model. *J. Chem. Phys.* **1999**, *110* (13), 6158–6170. https://doi.org/10.1063/1.478522.

(40) Krishnan, R.; Binkley, J. S.; Seeger, R.; Pople, J. A. Self-consistent Molecular Orbital Methods. XX. A Basis Set for Correlated Wave Functions. *The Journal of Chemical Physics* **2008**, *72* (1), 650–654. https://doi.org/10.1063/1.438955.

(41) Schmidt, K.; Brovelli, S.; Coropceanu, V.; Beljonne, D.; Cornil, J.; Bazzini, C.; Caronna, T.; Tubino, R.; Meinardi, F.; Shuai, Z.; Brédas, J.-L. Intersystem Crossing Processes in Nonplanar Aromatic Heterocyclic Molecules. *J. Phys. Chem. A* **2007**, *111* (42), 10490–10499. https://doi.org/10.1021/jp075248q.

(42) Guo, S.; Li, H. Photolysis of Nitrophenols in Gas Phase and Aqueous Environment: A Potential Daytime Source for Atmospheric Nitrous Acid (HONO). *Environ. Sci.: Atmos.* **2023**, *3* (1), 143–155. https://doi.org/10.1039/D2EA00053A.

(43) Furche, F.; Ahlrichs, R. Adiabatic Time-Dependent Density Functional Methods for Excited State Properties. *J. Chem. Phys.* **2002**, *117* (16), 7433–7447. https://doi.org/10.1063/1.1508368.

(44) Wang, J.; Durbeej, B. How Accurate Are TD-DFT Excited-State Geometries Compared to DFT Ground-State Geometries? *Journal of Computational Chemistry* **2020**, *41* (18), 1718–1729. https://doi.org/10.1002/jcc.26213.

(45) Quenneville, J.; Greenfield, M.; Moore, D. S.; McGrane, S. D.; Scharff, R. J. Quantum Chemistry Studies of Electronically Excited Nitrobenzene, TNA, and TNT. *J. Phys. Chem. A* **2011**, *115* (44), 12286–12297. https://doi.org/10.1021/jp204104j.

(46) Vogt, R. A.; Reichardt, C.; Crespo-Hernández, C. E. Excited-State Dynamics in Nitro-Naphthalene Derivatives: Intersystem Crossing to the Triplet Manifold in Hundreds of Femtoseconds. *J. Phys. Chem. A* **2013**, *117* (30), 6580–6588. https://doi.org/10.1021/jp405656n.

(47) Cammi, R.; Mennucci, B.; Tomasi, J. Fast Evaluation of Geometries and Properties of Excited Molecules in Solution: A Tamm-Dancoff Model with Application to 4-Dimethylaminobenzonitrile. *J. Phys. Chem. A* **2000**, *104* (23), 5631–5637. https://doi.org/10.1021/jp000156l.

(48) Wang, Y.-L.; Wu, G.-S. Improving the TDDFT Calculation of Low-Lying Excited States for Polycyclic Aromatic Hydrocarbons Using the Tamm–Dancoff Approximation. *International Journal of Quantum Chemistry* **2008**, *108* (3), 430–439. https://doi.org/10.1002/qua.21510.

(49) Risthaus, T.; Hansen, A.; Grimme, S. Excited States Using the Simplified Tamm–Dancoff-Approach for Range-Separated Hybrid Density Functionals: Development and Application. *Physical Chemistry Chemical Physics* **2014**, *16* (28), 14408–14419. https://doi.org/10.1039/C3CP54517B.

(50) Takezaki, M.; Hirota, N.; Terazima, M.; Sato, H.; Nakajima, T.; Kato, S. Geometries and Energies of Nitrobenzene Studied by CAS-SCF Calculations. *J. Phys. Chem. A* **1997**, *101* (28), 5190–5195. https://doi.org/10.1021/jp970937v.

(51) Crespo-Hernández, C. E.; Burdzinski, G.; Arce, R. Environmental Photochemistry of Nitro-PAHs: Direct Observation of Ultrafast Intersystem Crossing in 1-Nitropyrene. *J. Phys. Chem. A* **2008**, *112* (28), 6313–6319. https://doi.org/10.1021/jp803847q.

(52) Rafiq, S.; Yadav, R.; Sen, P. Femtosecond Excited-State Dynamics of 4-Nitrophenyl Pyrrolidinemethanol: Evidence of Twisted Intramolecular Charge Transfer and Intersystem Crossing Involving the Nitro Group. *J. Phys. Chem. A* **2011**, *115* (30), 8335–8343. https://doi.org/10.1021/jp2005524.

(53) El-Sayed, M. A. Spin—Orbit Coupling and the Radiationless Processes in Nitrogen Heterocyclics. *The Journal of Chemical Physics* **1963**, *38* (12), 2834–2838. https://doi.org/10.1063/1.1733610.

(54) Shizu, K.; Kaji, H. Theoretical Determination of Rate Constants from Excited States: Application to Benzophenone. *J. Phys. Chem. A* **2021**, *125* (40), 9000–9010. https://doi.org/10.1021/acs.jpca.1c06165.

(55) Marian, C. M. Understanding and Controlling Intersystem Crossing in Molecules. *Annual Review of Physical Chemistry* **2021**, *72* (1), 617–640. https://doi.org/10.1146/annurev-physchem-061020-053433.

(56) Sousa, C.; Domingo, A.; de Graaf, C. Effect of Second-Order Spin–Orbit Coupling on the Interaction between Spin States in Spin-Crossover Systems. *Chemistry – A European Journal* **2018**, *24* (20), 5146–5152. https://doi.org/10.1002/chem.201704854.

(57) Penfold, T. J.; Gindensperger, E.; Daniel, C.; Marian, C. M. Spin-Vibronic Mechanism for Intersystem Crossing. *Chem. Rev.* **2018**, *118* (15), 6975–7025. https://doi.org/10.1021/acs.chemrev.7b00617.

(58) Yanai, T.; Tew, D. P.; Handy, N. C. A New Hybrid Exchange–Correlation Functional Using the Coulomb-Attenuating Method (CAM-B3LYP). *Chemical Physics Letters* **2004**, *393* (1), 51–57. https://doi.org/10.1016/j.cplett.2004.06.011.

(59) Kobayashi, R.; Amos, R. D. The Application of CAM-B3LYP to the Charge-Transfer Band Problem of the Zincbacteriochlorin–Bacteriochlorin Complex. *Chemical Physics Letters* **2006**, *420* (1), 106–109. https://doi.org/10.1016/j.cplett.2005.12.040.

(60) Komjáti, B.; Urai, Á.; Hosztafi, S.; Kökösi, J.; Kováts, B.; Nagy, J.; Horváth, P. Systematic Study on the TD-DFT Calculated Electronic Circular Dichroism Spectra of Chiral Aromatic Nitro Compounds: A Comparison of B3LYP and CAM-B3LYP. *Spectrochimica Acta Part A: Molecular and Biomolecular Spectroscopy* **2016**, *155*, 95–102. https://doi.org/10.1016/j.saa.2015.11.002.

(61) Pines, E.; Pines, D.; Barak, T.; Magnes, B.-Z.; Tolbert, L. M.; Haubrich, J. E. Isotope and Temperature Effects in Ultrafast Proton-Transfer from a Strong Excited-State Acid. *Berichte der Bunsengesellschaft für physikalische Chemie* **1998**, *102* (3), 511–517. https://doi.org/10.1002/bbpc.19981020334.

(62) Arnaut, L. G.; Formosinho, S. J. Excited-State Proton Transfer Reactions I. Fundamentals and Intermolecular Reactions. *Journal of Photochemistry and Photobiology A: Chemistry* **1993**, *75* (1), 1–20. https://doi.org/10.1016/1010-6030(93)80157-5.

(63) Tolbert, L. M.; Solntsev, K. M. Excited-State Proton Transfer: From Constrained Systems to "Super" Photoacids to Superfast Proton Transfer. *Acc. Chem. Res.* **2002**, *35* (1), 19–27. https://doi.org/10.1021/ar990109f.

(64) Simkovitch, R.; Karton-Lifshin, N.; Shomer, S.; Shabat, D.; Huppert, D. Ultrafast Excited-State Proton Transfer to the Solvent Occurs on a Hundred-Femtosecond Time-Scale. *J. Phys. Chem. A* **2013**, *117* (16), 3405–3413. https://doi.org/10.1021/jp4014724.

(65) Alif, A.; Pilichowski, J.-F.; Boule, P. Photochemistry and Environment XIII: Phototransformation of 2-Nitrophenol in Aqueous Solution. *Journal of Photochemistry and Photobiology A: Chemistry* **1991**, *59* (2), 209–219. https://doi.org/10.1016/1010-6030(91)87009-K.

(66) Dubowski, Y.; Hoffmann, M. R. Photochemical Transformations in Ice: Implications for the Fate of Chemical Species. *Geophysical Research Letters* **2000**, *27* (20), 3321–3324. https://doi.org/10.1029/2000GL011701.

TOC Graphic